Materials & Design 221 (2022) 110923

Contents lists available at ScienceDirect

Materials & Design

journal homepage: www.elsevier.com/locate/matdes

The near-isotropic elastic properties of interpenetrating composites reinforced by regular fibre-networks

Zhengyang Zhang [a,b], Hanxing Zhu [a,*], Ru Yuan [c], Sanmin Wang [c], Tongxiang Fan [d], Yacine Rezgui [a], Di Zhang [d]

[a] School of Engineering, Cardiff University, Cardiff CF24 3AA, UK
[b] UM-SJTU Joint Institute, Shanghai Jiaotong University, Shanghai 200240, China
[c] School of Mechanical Engineering, Northwestern Polytechnical University, Xi'an 710072, China
[d] State Key Lab of Metal Matrix Composites, School of Materials Science and Engineering, Shanghai Jiao Tong University, Shanghai 200240, PR China

HIGHLIGHTS

- All IPCs can have an almost isotropic Young's modulus larger than the Voigt limit.
- The range and largest values of the normalised Young's moduli of the IPCs are identified.
- Structural hierarchy of the IPCs can enhance their stiffness.

GRAPHICAL ABSTRACT

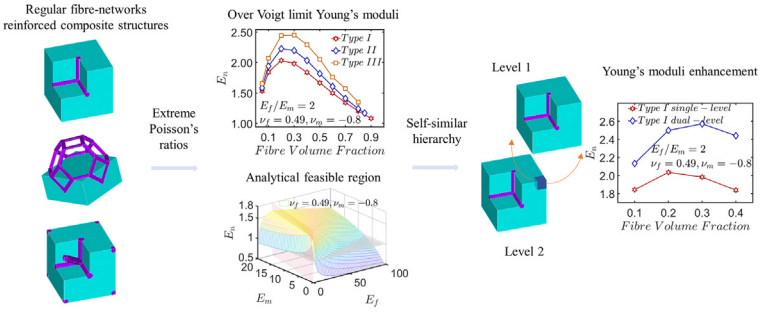

ARTICLE INFO

Article history:
Received 13 November 2021
Revised 3 July 2022
Accepted 3 July 2022
Available online 14 July 2022

Keywords:
Interpenetrating phase composites
Elastic properties
Finite element simulation
Structural hierarchy

ABSTRACT

It is highly demanding and challenging to maximise the stiffness of the interpenetrating phase composites (IPCs) while still keeping their isotropy. In this paper, the elastic properties of IPCs reinforced by three different types of regular lattice fibre networks are investigated by computer simulation and analytical methods. The numerical results indicate that the larger the difference between the Poisson's ratios and the smaller the difference between the Young's moduli of the constituent materials, the larger the Young's moduli of these IPCs are. It is also found that structural hierarchy can enhance the stiffness of these IPCs by 30%. In addition, the three types of IPCs have Zener anisotropy factors in the range of 1.0 ± 0.04 in most cases, could have an almost isotropic Young's modulus two times larger than the Voigt limit, and a Poisson's ratio with a positive or negative or zero value. Moreover, they are easy to manufacture, their Young's moduli are in general 1.0–3.0 times those of the conventional particle or short fibre reinforced composites and other types of IPCs including those reinforced by the triply periodic minimal surface (TPMS) shells, and the type of IPCs with the largest Young's modulus has been identified.

1. Introduction

Interpenetrating phase composites (IPCs) are a class of composites in which the constituent phases are continuous in their geometry and each phase is interconnected in terms of its architecture or microstructure to bear loads independently and hold the completeness of the structure, even if the other phases of the compos-

* Corresponding author.
E-mail address: zhuh3@cardiff.ac.uk (H. Zhu).

https://doi.org/10.1016/j.matdes.2022.110923

ites fail [1]. The co-continuous structure of all the phases provides the IPCs with various advantages in tuneable stiffness, strength, coefficient of thermal expansion, high impact resistance and enhanced ionic conductivity [2–11], compared to their conventional, discretely reinforced counterparts, such as particle, whisker or unidirectional fibre reinforced composites [12–17]. IPCs reinforced by a regular cubic or body centred cubic open-cell foam structure have been studied by experimental measurements [10,18,19], finite element (FE) simulation [20,21] and molecular dynamics [7]. The effects of the constituent materials' mechanical properties, however, have not been systematically considered. Foam based IPCs have been manufactured and found to be much stiffer and stronger than those of the constituent foams [22]. Triply periodic minimal surfaces (TPMS) are also regarded as promising reinforcement structures for IPCs [23–25] and experimental results indicated that the mechanical properties of the TPMS reinforced IPCs were much better than those of the IPCs with the idealized Schoen's I-WP reinforcement structures at 15% volume fraction [23,25]. However, this conclusion may need further consideration as the connecting parts of the idealized reinforcement structure are composed of sharp connection edges, which is not considered a well-designed structure.

Notably, it has been found that the Young's Modulus of an almost isotropic composite can significantly exceed the Voigt limit [26,27], which had long been regarded as an unreachable limit of the stiffness of isotropic composite materials. Moreover, the Poisson's ratio of IPCs was proved to be tuneable to any desired value, e.g. positive, or negative, or zero when using special matrix material or specifically designed auxetic reinforcement structures [26–29]. Analytical approach and FE simulation also showed that in addition to the superior mechanical properties, IPCs also performed well in terms of their thermal and electrical conductivities [30].

In general, the factors which affect the mechanical properties of composites include the geometrical structure, mechanical properties of the constituent materials (such as Poisson's ratios, Young's moduli), interphase conditions between reinforcement and matrix [27,31]. Identical periodic cells, including cubic, and body-centred-cubic (BCC or tetrakaidekahedral) cells have been widely used to simulate the reinforcement structure of IPCs [20,21,27,32,33]. However, very little effort has been made to explore the combined effects of the micro-scale structure and the mechanical properties of the constituent phases on the effective mechanical properties of the IPCs.

This paper aims to perform numerical simulations to investigate these effects on the elastic properties of IPCs with different types of geometric structures of the reinforcement phase, and to achieve an almost isotropic Young's modulus much larger than the Voigt limit. In addition, an analytical approach will be introduced to determine the normalised Young' s moduli of the composites within the feasible design space of the Young's moduli and Poisson's ratios of the constituent materials. The results obtained in this paper will be compared to the relevant experimental and simulation results of IPCs and conventional composites, and the IPC with the largest and almost isotropic dimensionless Young's modulus will be identified. The IPCs studied in this paper can have a size from macro scale down to micro or nano scale, and they have applications in most engineering structures.

2. Geometric structures and computational methods

2.1. Geometric structures

This paper focuses on the two-phase interpenetrating composites made of two homogeneous and isotropic constituent materials. Thus, the reinforcement structure in a two-phase IPC is a kind of open cell foam. As simple and easily manufacturable structures, three types of reinforcement fibre network structures are considered: (I) cross-cubic, (II) cross-cubic with space diagonals, (III) tetrakaidekahedral. All the reinforcement fibres are assumed to have the same uniform circular cross-section and the matrix phase completely and perfectly fills the porous space of the fibre-network (i.e. there is no interlayer or defect between the fibres and the matrix). Logically, the stiffer the reinforcement lattice structure, the larger the stiffness of the IPC. Obviously, the cross-cubic lattice has the largest nearly isotropic Young's modulus among all different types of open cell foams (fibre-networks), but the BCC and cross-cubic lattice with space diagonals have better isotropy. Moreover, all these three types of reinforcement fibre networks are easy to produce compared to other perfect regular open cell structures such as TPMS.

Representative volume elements (RVEs) are usually used to model the mechanical properties of composites [34]. RVE models should be sufficiently small to reduce the calculation time and sufficiently large to include all the features and characteristics of the structure to represent the target material. As all three types of IPCs have periodic structures, periodic RVE models and periodic boundary conditions are used to simulate their mechanical properties, as shown in Fig. 1. The material in cyan colour represents the matrix while the material in purple colour represents the reinforcement fibre networks.

All three types of cubic RVEs are assumed to have the same edge length L, the Young's moduli and Poisson's ratios of the constituent materials (i.e. matrix and fibre-network) are denoted as E_m, E_f, v_m and v_f, respectively. In order to compare their effective elastic properties, the three different types of IPCs are assumed to have the same volume fraction of the reinforcement fibre network material V_f. To make it easier to partition the reinforcement fibre-network into tetrahedral elements, the intersections of the fibres are represented by the smallest possible spheres that can enclose the intersection lines between the connected fibres. As the IPCs are made of only two constituent materials, it is obvious that $V_f + V_m = 1$. The volume fractions of the reinforcement fibre network structures considered in this study range from 3% to nearly the geometrical upper limit of each type of the structures. The fibre diameters of the three types of reinforcement fibre networks d_I, d_{II} and d_{III} should thus satisfy the following relations:

$$d_I < L\# \tag{1}$$

$$d_{II} < \frac{\sqrt{2}}{1+\sqrt{3}} L\# \tag{2}$$

$$d_{III} < \frac{\sqrt{6}}{8} L\# \tag{3}$$

where L is the edge length of the corresponding cubic RVE model.

Thus, the maximum fibre volume fractions (i.e. upper limits) of the three types of IPCs considered in this study are given below in Table 1. It should be noted that if the fibre volume fraction is too small, the total number of elements of the RVE model would be too large, which would be significantly increase the computational cost.

When the volume fractions of the reinforcement fibre networks approach their upper limits, the corresponding matrix structures of the three types of IPCs are shown below in Fig. 2.

2.2. Model parameters

In order to explore how the elastic properties of the IPCs are affected by those of their constituent materials and volume fractions, the Young's moduli and Poisson's ratios of the constituent materials should be in reasonable ranges.

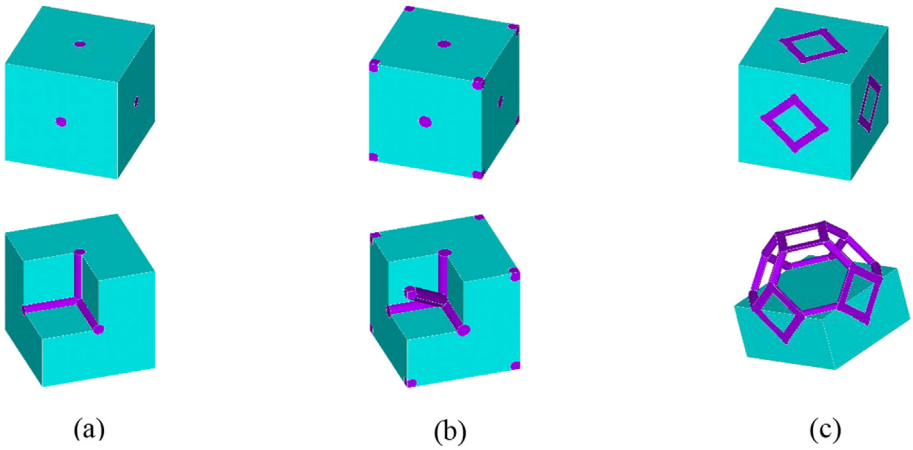

Fig. 1. Periodic RVE models of IPCs reinforced by three different types of self-connected regular fibre networks: (a) Type I, (b) Type II, (c) Type III.

Table 1
Fibre volume fractions of different types of composite structures.

	Min Volume fraction	Max Volume fraction
Type I	3%	90%
Type II	3%	85%
Type III	3%	80%

The Young's moduli of most metals, alloys, ceramics and carbon fibres are in the range between 60 and 400 GPa; and most solid polymers have a Young's modulus from 0.1 to 10 GPa [35]. In most metal matrix composites reinforced by a metal or ceramic, the ratio E_f/E_m stays in the range from 2 to 10, e.g. Al/Al_2O_3 IPCs [36]. In this paper, the Young's modulus of the matrix material is assumed to be $E_m = 1$, thus the Young's modulus of the fibre-network material is $E_f = E_f|_{actual}/E_m|_{actual}$, and the obtained effective Young's modulus of the IPC, E_c, is a dimensionless modulus which has already been normalised by the Young's modulus of the matrix material.

Although the possible Poisson's ratios of isotropic materials are in the domain $(-1, 0.5)$, most natural materials have a positive Poisson's ratio. For example, cork's Poisson's ratio is very close to 0 [37]; Beryllium and Boron are close on the periodic table and have similar Poisson's ratio between 0.02 and 0.1 [38]; Bones have a Poisson's ratio from 0.1 to 0.2, woods are anisotropic materials with a directional Poisson's ratio from 0.2 to 0.4; and the Poisson's ratios of metals such as iron, aluminium and copper lie in the interval of (0.2, 0.4). When it comes to synthetic or fabricated isotropic materials, however, the range of their Poisson's ratios is significantly widened. Solid polymer/rubber and low density regular or irregular open cell foams have a Poisson's ratio close to the upper limit 0.5 [39,40]; modern carbon fibre fabrications and their composites can have a Poisson's ratio from 0.02 to negative [38]; re-entrant foams [41], auxetic composites can have an isotropic Poisson's ratio close to -1.0 [35].

In the simulations of this paper, $E_f/E_m = 2$ is for two similar constituent phases (e.g. metal-ceramic IPCs) and $E_f/E_m = 10$ is for two constituent phases with some larger difference in Young's moduli (such as polymer-aluminium or resin-glass IPCs). It has been found that the Young's moduli of an almost isotropic composite could be tuned to surpass the Voigt limit with disparate Poisson's ratios [26,27]. Thus, v_m and v_f are set to be as different as possible within the possible range of isotropic materials to show the effect of Poisson's ratios of the constituent materials on the elastic performance of the IPCs. Based on the above discussion, the possible values of E_m, E_f, v_m and v_f of the constituent materials of the IPCs are given in Table 2.

2.3. Computational method

The RVE models of the IPCs reinforced by the three different types of fibre-networks as shown in Fig. 1 are constructed in ANSYS software [42]. Both the fibre and matrix in each RVE model are discretized by solid 187 tetrahedral elements. As all three types of IPCs are periodic, periodic boundary conditions are applied to the RVE models in the finite element simulations. To obtain the effective Young's modulus E_{xx} and Poisson's ratio v_{xy} of the IPCs,

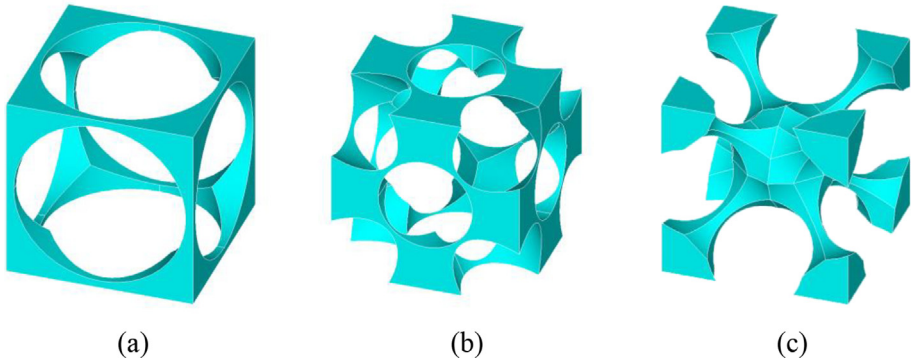

Fig. 2. The corresponding matrix structures in the RVEs when their fibre volume fractions approach their upper limits.

Table 2
Young's moduli and Poisson's ratios of the constituent materials.

E_f/E_m	2	10
v_f	0.05	0.49
v_m	−0.8	0.49

a tensile strain of 0.1% is applied to the RVE models in the [100] direction in the simulations.

3. Results

The focus of this study is to investigate how the elastic properties of the IPCs depend on the geometrical structure and the volume fraction of the reinforcement fibre-network, and the combination of the elastic properties of the two constituent materials. As all three types of RVEs have cubic symmetry, the IPCs have only three independent elastic constants [39] to be determined, namely E_{xx}, G_{xy} and v_{xy}. Further, the factor of their anisotropy will be evaluated.

3.1. The normalised Young's moduli of IPCs

To study how the elastic properties of these IPCs depend on those of their constituent materials, six different combinations of the elastic properties of their constituent materials are considered and given in Table 3. For the convenience to compare the Young's moduli of the IPCs with those of other composite materials, the Young's moduli of the IPCs are normalised by the Voigt limit and expressed as

$$E_n = E_c/E_{cVoigt}\# \tag{4}$$

where $E_{cVoigt} = E_f V_f + E_m V_m$.

For different combinations of the constituent materials given in Table 3, Fig. 3 presents the comparison of the normalised Young's moduli of the three types of IPCs. The broken horizontal line with a dimensionless value of 1.0 stands for the Voigt limit normalised by itself. Thus, the results plotted above this line indicates that the Young's modulus of the IPC E_c is larger than the Voigt limit.

As can be seen from Fig. 3, the normalised Young's moduli E_n of the IPCs decrease, reach their lower limits, and then increase with the increase of the fibre volume fraction when both v_f and v_m are positive. Most of the values of the normalised Young's moduli of the IPCs, E_n, are smaller than 1, indicating that the Young's moduli of the IPCs are smaller than the Voigt limit. However, when v_f is positive and v_m is negative, the normalised Young's moduli of the IPCs increase first, reach their peaks, and then decrease with the increase of the fibre volume fraction as can be seen in Fig. 3(c) and (d). E_n is larger than 1 in most of the fibre volume fraction range and can be significantly larger than 2.0 in some conditions. Fig. 3(c) shows that for IPCs with $E_f/E_m = 2$ and the Poisson's ratio of their matrix being negative, their largest normalised Young's modulus can be obtained when the fibre volume fraction V_f is between 20% and 30%. For similar IPCs with $E_f/E_m = 10$, Fig. 3(d) indicates that the largest normalised Young's modulus can be achieved when the fibre volume fraction V_f is around 10–15%.

In general, E_n increases with E_f/E_m approaching 1 and with the increase of $|v_f - v_m|$. The normalised Young's modulus of the type I IPC is larger than those of the other two types of IPCs when the Poisson's ratios of both the two constituent materials are positive. However, when the difference of Poisson's ratios of the two constituent materials is large (i.e. v_f is positive and v_m is negative), the normalised Young's modulus of the type III IPC is larger than that of the type II, and the latter is larger than the type I in most of the cases. The possible reason is that the much larger stiffness of the type-I reinforcement fibre network (i.e. 'open cell foam') dominates the stiffness of the IPC when the difference of Poisson's ratios of the two constituent materials is small. When the difference of Poisson's ratios of the two constituent materials is large, the stresses and strains in the type-III IPC are more non-uniform, and the much higher stress and strain concentration in the type-III IPC results in larger stored strain energy density and consequently larger stiffness of the IPC. This finding may provide a guideline for designing new lattice reinforced IPCs with the possible largest and almost isotropic stiffness. Thus, the largest stiffness of almost isotropic IPCs depends on the interplay among the stiffness of the reinforcement fibre-network ('open cell foam'), the combination of the constituent material properties, and the stress and strain concentration level.

Here the extreme negative Poisson's ratios of matrix materials are selected to test the structures which are hard to find in common non-porous materials. However, it has been demonstrated that with materials of easy-access and proper reinforcement structures, the Poisson's ratio of solid composites can be designed to be either positive, or negative, or zero [28]. It is possible to use these structures as the matrix in all three types of IPCs in this work. For example, the type-I solid auxetic structure (composite) of reference [28] (as shown in Fig. 4(a)) can be used as the matrix of the type-I IPCs in this paper (as shown in Fig. 4(b)). The type-I solid auxetic structure (composite) in reference [28] can reach a Poisson's ratio of −0.4 with proper solid constituent materials. Fig. 4 (c) demonstrates that the normalised Young's modulus of the type-I IPCs with their matrix being a solid auxetic composite can be larger than the Voigt limit.

Table 3
Parameters of the constituent materials used in comparison of the normalised Young's moduli of type I, II and III IPCs.

	$v_f = 0.49$, $v_m = 0.05$	$v_f = 0.49$, $v_m = -0.8$	$v_f = 0.3$, $v_m = 0.3$
$E_f/E_m = 2$	Fig. 3(a)	Fig. 3(c)	Fig. 3(e)
$E_f/E_m = 10$	Fig. 3(b)	Fig. 3(d)	Fig. 3(f)

3.2. The Poisson's ratio of the IPCs

Fig. 5. shows the effects of fibre volume fraction on the Poisson's ratios of different types of IPCs with different combinations of the constituent material properties. As can be seen, there is no obvious difference between the Poisson's ratios of these three different types of IPCs, and they all can be positive, negative or zero depending on the constituent material properties and the fibre volume fraction. Although a negative Poisson's ratio cannot be achieved by the three types of IPCs studied here when the Poisson's ratios of both the constituent materials are positive, the effective Young's moduli of these IPCs are much larger than those of the auxetic IPCs [28].

3.3. The anisotropy factors of the IPCs

As all three types of the IPCs have cubic symmetry, they have only three independent elastic constants and the anisotropy factor can be expressed as [39]

$$A = \frac{2(S_{11}-S_{12})}{S_{44}} = \frac{2(1+v_{xy})G_{xy}}{E_{xx}}\# \tag{5}$$

where S_{ij} denote the components of the compliance matrix, v_{xy} represents the Poisson's ratio, G_{xy} the shear modulus and E_{xx} the Young's modulus of the IPCs. The Young's moduli and Poisson's

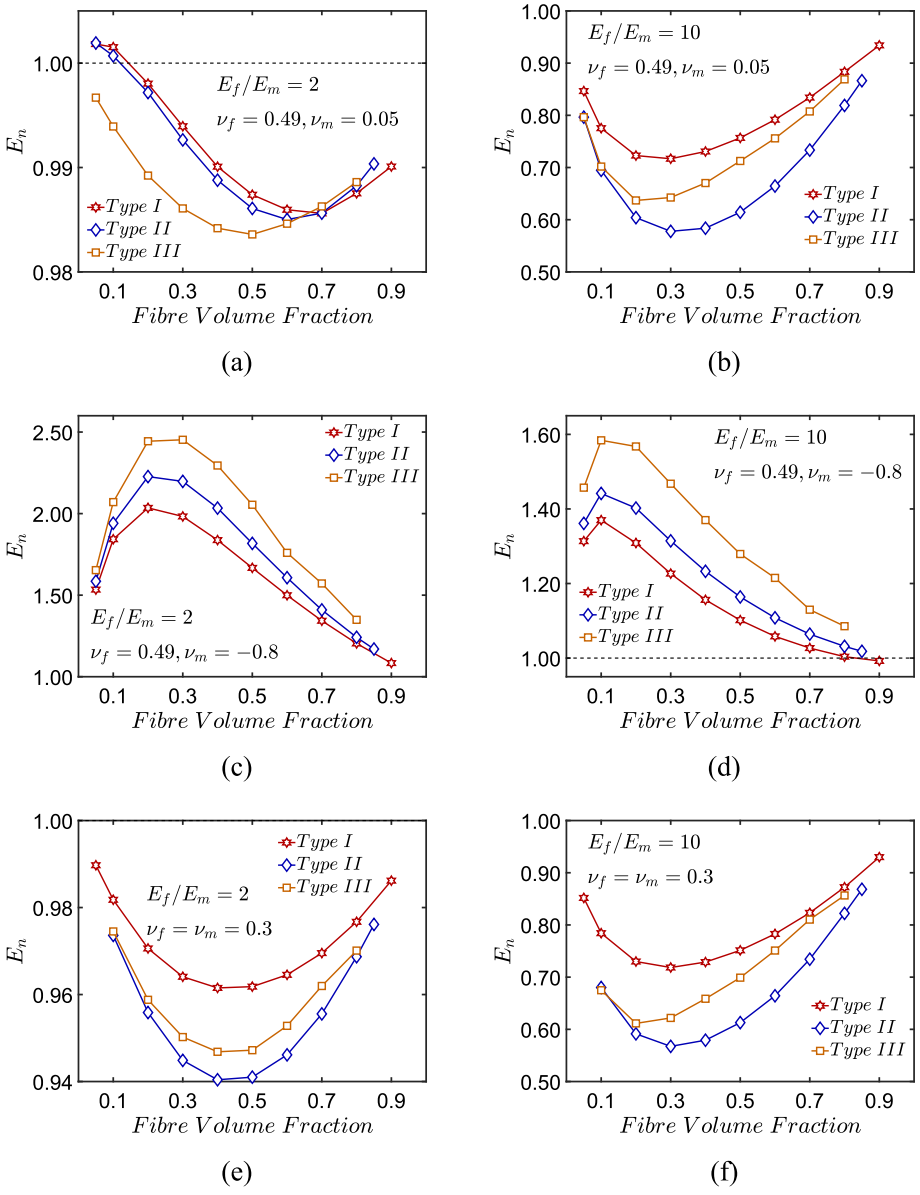

Fig. 3. Comparison of the normalised Young's moduli of the three types of IPCs with different combinations of constituent material properties.

ratios of the three types of IPCs are obtained and presented in Figs. 3 and 5, and their shear moduli are also obtained by simulations. As the shear moduli of the three types of IPCs are similar to their Young's moduli shown in Fig. 3 and the main difference is their magnitudes, the results are not presented here. Thus, their anisotropy factors can be obtained from Equation (5) and the results are shown in Fig. 6. As can be seen, the anisotropy factors of the three types of IPCs are very close to 1.0 except for the case with the constituent material properties shown in Fig. 6(b). Therefore, the elastic properties of all three types of IPCs are almost isotropic in most cases, e.g. the cases with the difference between the Young's moduli of the two constituent materials not being too large as shown in Fig. 6(a) and (c).

3.4. The feasible design space of the IPCs

The Young's modulus E_{xx} and Poisson's ratio v_{xy} of the IPCs reinforced by a cubic fibre-network can be theoretically obtained by solving a set of linear equations [27]. To simplify the analysis, the reinforcement fibres are assumed to have a uniform square cross section of side length T. The analytical results of the normalised Young's moduli E_n of the type I IPCs can be obtained by solving a set of simultaneous equations given in appendix 1.

Fig. 3(c) indicates that the type I IPC with cylinder fibres can achieve a maximum normalised Young's modulus when the fibre volume fraction $V_f = 0.2$. The same value is selected in the theoretical analyse in this section. Thus $T/L \approx 0.28714$ is obtained from $V_f = \left(3LT^2 - 2T^3\right)/L^3 = 0.2$. Confining the Poisson's ratio of the fibre material v_f to (0, 0.5) and that of the matrix v_m to (−1, 0.5), the effects of v_f, v_m on the normalisedYoung's moduli of the type I IPCs with a fixed fibre volume fraction $V_f = 0.2$ and different ratios $E_f/E_m = 2$ and $E_f/E_m = 10$ can be analytically obtained and shown in Fig. 7, where the grey horizontal plane represents the normalised Voigt limit E_V.

Furthermore, if the Young's modulus of the fibre material E_f varies from 1 to 100 and that of the matrix E_m varies from 1 to 10, the effects of E_f and E_m on the normalised Young's moduli (i.e. normalised by the Voigt limit and obtained by the analytic method) of the type I IPCs with the fixed fibre volume fraction $V_f = 0.2$

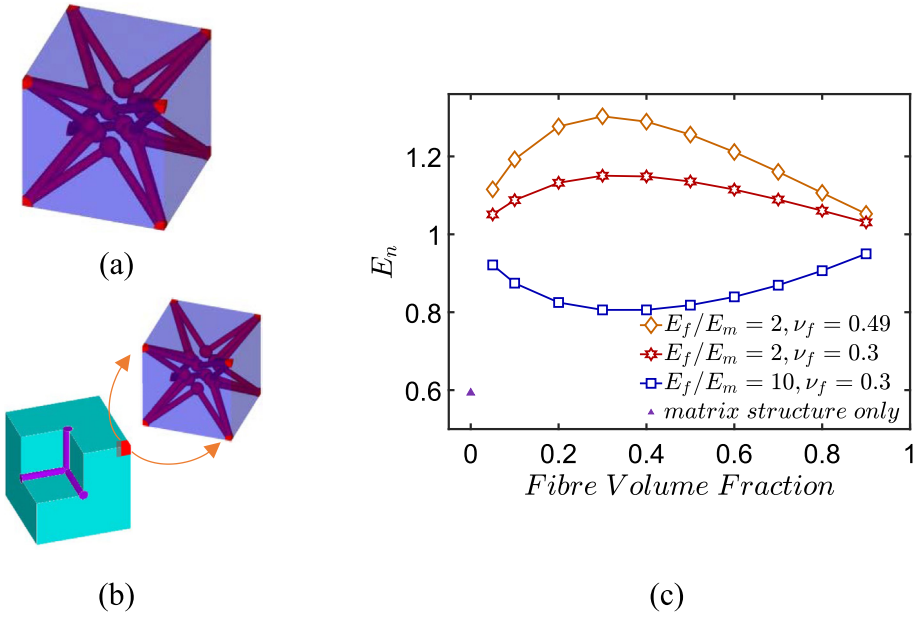

Fig. 4. (a) The solid auxetic composite with a negative Poisson's ratio [28], (b) the type-I IPC with its matrix being made of the solid auxetic composite, (c) demonstration of the type-I composites with their Young's moduli larger than the Voigt limit.

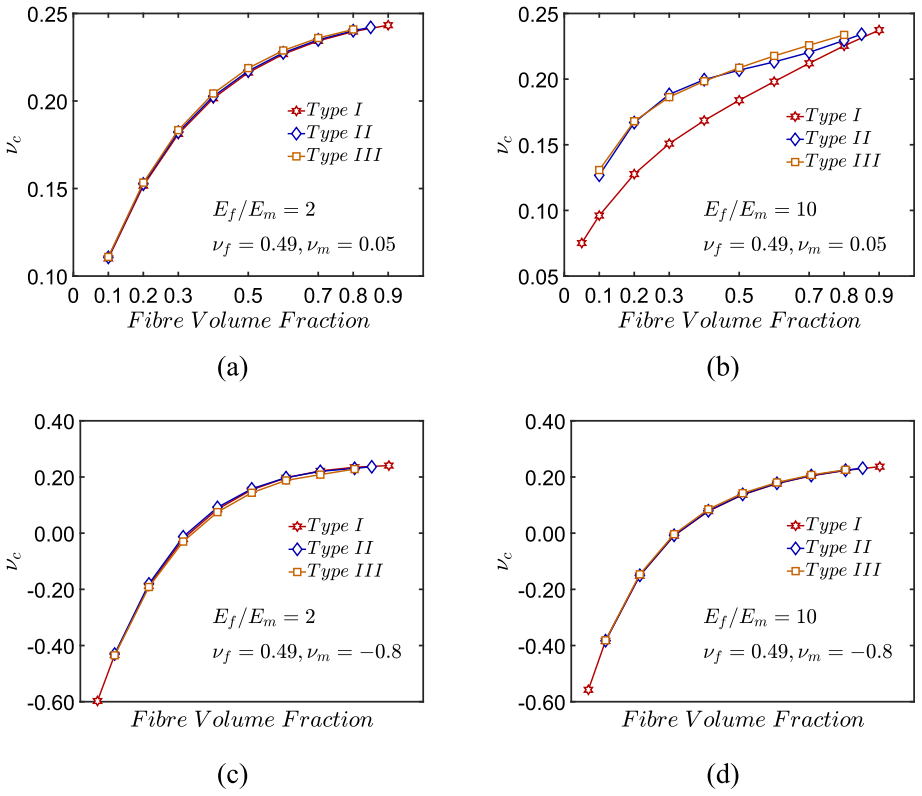

Fig. 5. Comparison of the Poisson's ratios of the three types of IPCs with different combinations of the constituent material properties.

and two different combinations of the Poisson's ratios of their constituent materials $v_f = v_m = 0.3$ and $v_f = 0.49$, $v_m = -0.8$ are illustrated in Fig. 8, where the grey horizontal plane represents the normalised Voigt limit E_V and the pink vertical plane represents the cases when $E_m = E_f$. Obviously, the closer the Young's moduli of the two constituent materials E_m and E_f, the larger the effects of the Poisson's ratios of the constituent materials on the normalised Young's moduli of the IPCs, and the IPCs have the largest normalised Young's moduli when $E_m = E_f$.

3.5. The self-similar hierarchical structure of IPCs

All the IPC structures presented in this paper have the potential to form self-similar hierarchical structures to further tune their mechanical properties. Here a two level self-similar hierarchy

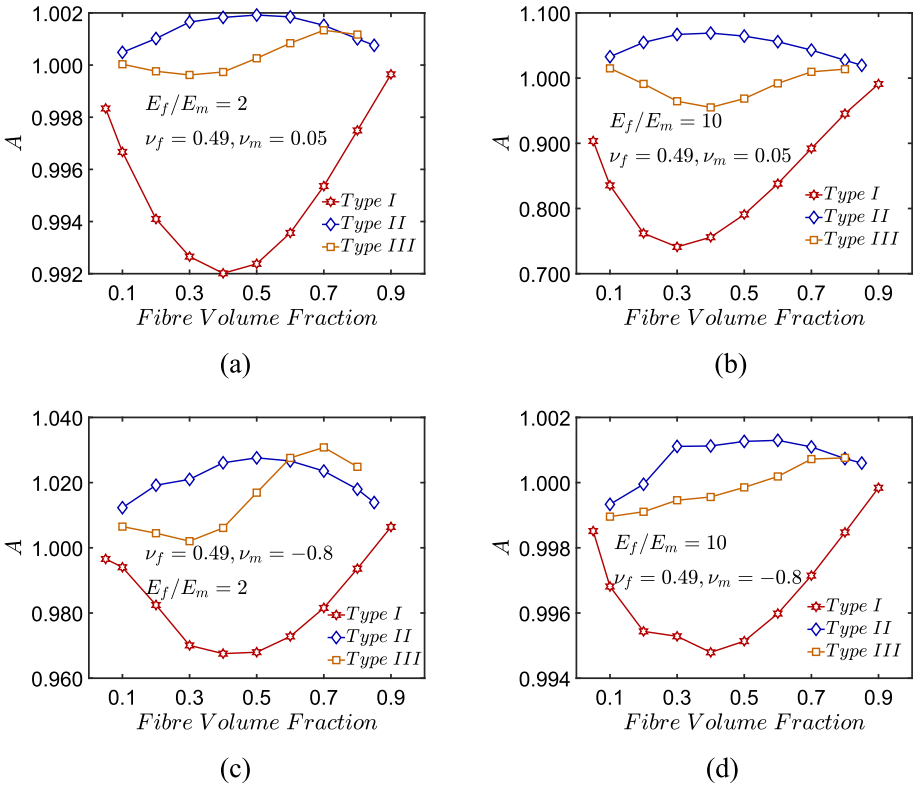

Fig. 6. Comparison of the anisotropy factors A of the three types of IPCs with different combinations of the constituent material properties.

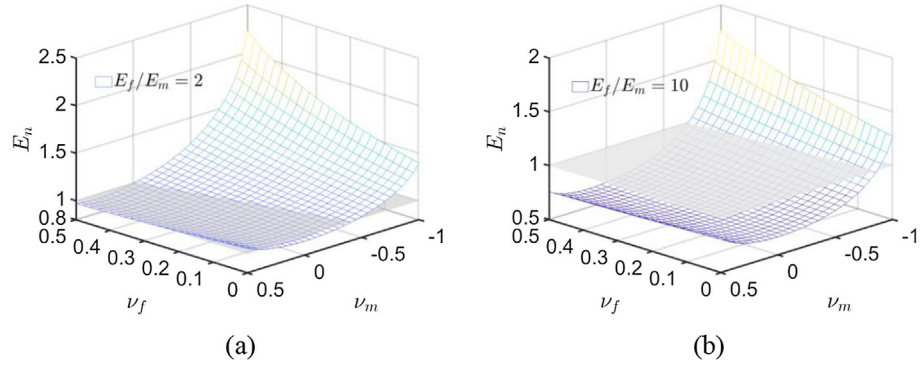

Fig. 7. Effects of v_f and v_m on the normalised Young's moduli E_n of the type I IPCs with a fixed volume fraction $V_f = 0.2$: (a) $E_f/E_m = 2$; (b) $E_f/E_m = 10$.

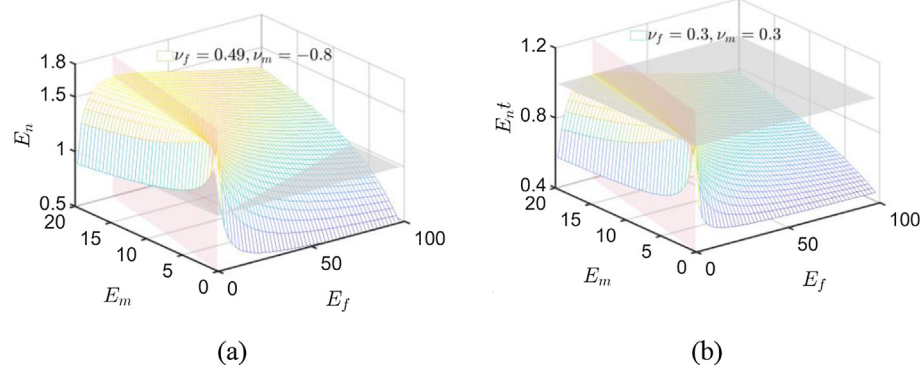

Fig. 8. Effects of E_f and E_m on the normalised Young's moduli of the type I IPCs with a fixed fibre volume fraction $V_f = 0.2$: (a)$v_f = 0.49$; $v_m = -0.8$. (b) $v_f = v_m = 0.3$.

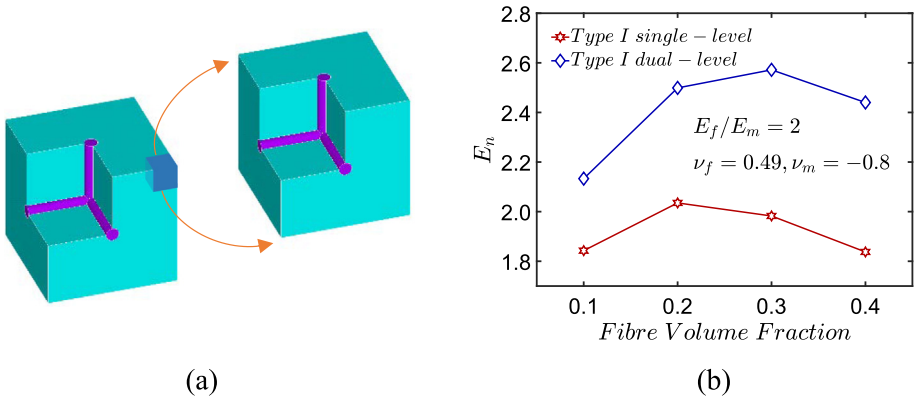

Fig. 9. Effects of self-similar structural hierarchy on the Young's moduli of the type I IPCs with different fibre volume fractions $V_f = 0.1, 0.2, 0.3, 0.4$. (a) schematic illustration of the hierarchical structure; (b) the enhancement of the Young's modulus by structural hierarchy.

based on Type I IPC structure has been designed as shown in Fig. 9 (a). The first level composite is made of two component materials with $E_f = 2.0$, $v_f = 0.49$, $E_m = 1.0$, $v_m = -0.8$ and the first level IPC acts as the matrix of the second level, the reinforcement material of the second level is the same as that of the first level. For the self-similarity, the fibre volume fraction of the second level V_{f2} and the first level V_{f1} are the same, thus $V_{f1} = V_{f2} = 1 - \sqrt{1 - V_f}$. Fig. 9(b) shows the comparison between the elastic moduli of the hierarchical IPCs and the single-level IPCs with the same total fibre volume fractions. As can be seen, structural hierarchy can significantly enhance the normalised Young's moduli of the IPCs.

4. Discussion

As the traditional particle composites and unidirectional fibre reinforced composites have been well investigated, it is necessary to compare the elastic properties of the lattice structured IPCs in this paper to those of the conventional counterparts. Chawla et al. [43] have done both experimental measurements and computational simulation on the elastic properties of SiC/Aluminium particle composites. Dekkers and Heikens [44] have tested the tensile behaviour of polystyrene-glass-bead composites. Rousseau and Tippur have studied the fracture behaviour of compositionally graded epoxy based glass particle composites [45]. Comparing the conventional composites to the IPCs could prove that reinforcement with a self-connected phase significantly enhances the elastic properties of IPCs with the same constituent materials and fibre volume fraction. The elastic properties of the constituent materials in the conventional particle reinforced composites in the reference papers [43–45] are listed in Table 4, and their reinforcement volume fractions are listed in Table 5.

Fig. 10 shows the comparison between the normalised Young's moduli of the IPCs reinforced by the three types of regular fibre-networks in this paper and those of the particle composites in the reference papers [43–45]. As can be seen, the three types of IPCs in general have a normalised Young's modulus larger than those of the particle composites.

Although IPCs can be fabricated via different methods [22,23,32,36] as shown in Fig. 11, however, it is hard to fabricate IPCs, especially those whose reinforcement phase is a well-connected lattice (or a regular) structure. Thus, the relevant experimental samples and results in literature often lack the comprehensiveness for exploring their superior mechanical properties. Here, the relevant experimental and numerical results of the IPCs in literature [22,23,32,36] are compared with the simulation results of the IPCs in this paper. The elastic properties and the volume fractions of the constituent materials in the IPCs in literature are listed in Table 6, and the normalised Young's moduli of those IPCs are compared with our results in Table 7 and Fig. 12.

As can be seen from Table 7, the Young's moduli of the IPCs in this paper are better than those of the IPCs fabricated with syntactic foam [22,32], the alumina-aluminium composites [36], and the TPMS-IPCs [23] which are relatively difficult to fabricate with metals like aluminum or steel. Al-ketan *et al* [23] have used 3D printing to manufacture periodic IPCs reinforced by four different types of

Table 4
Summary of particle reinforced composites used for comparison with our models.

Composites	E_f(MPa)	v_f	E_m(MPa)	v_m
SiC /Al [43]*	410,000	0.19	74,000	0.33
Glass/Polystyrene [44]	70,000	0.22	3250	0.34
Glass /Epoxy [45]**	69,000	0.15	3000	0.35

*Computational results from Ref. [43] are taken for comparison.
**Experimental results from Ref. [45] are taken for comparison.

Table 5
Reinforcement volume fractions of the particle reinforced composites in reference papers.

Composites	Reinforcement volume fractions				
SiC/Al [43]	10%	20%			30%
Glass/Polystyrene [44]	10%	15%		20%	25%
Glass/Epoxy [45]	14%	22%	28%	35%	43%

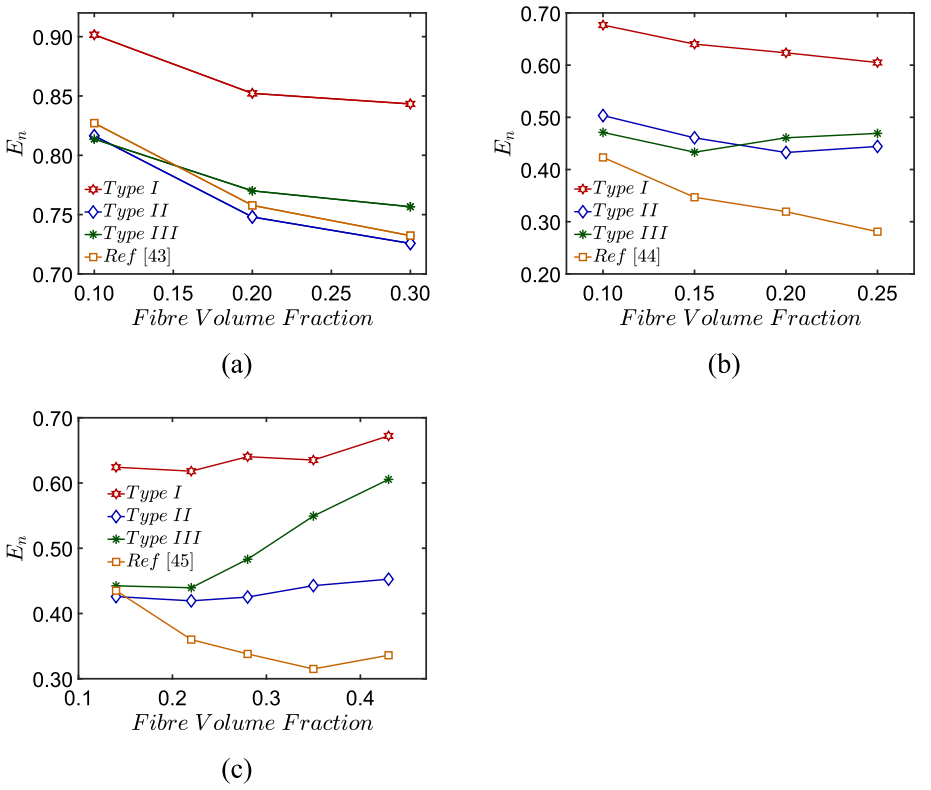

Fig. 10. Comparison between the normalised Young's moduli of the three types of structured IPCs and those of the traditional particle composites in literature: (a) the computational results in [43], (b) experimental results in [44] and (c) the experimental results in [45].

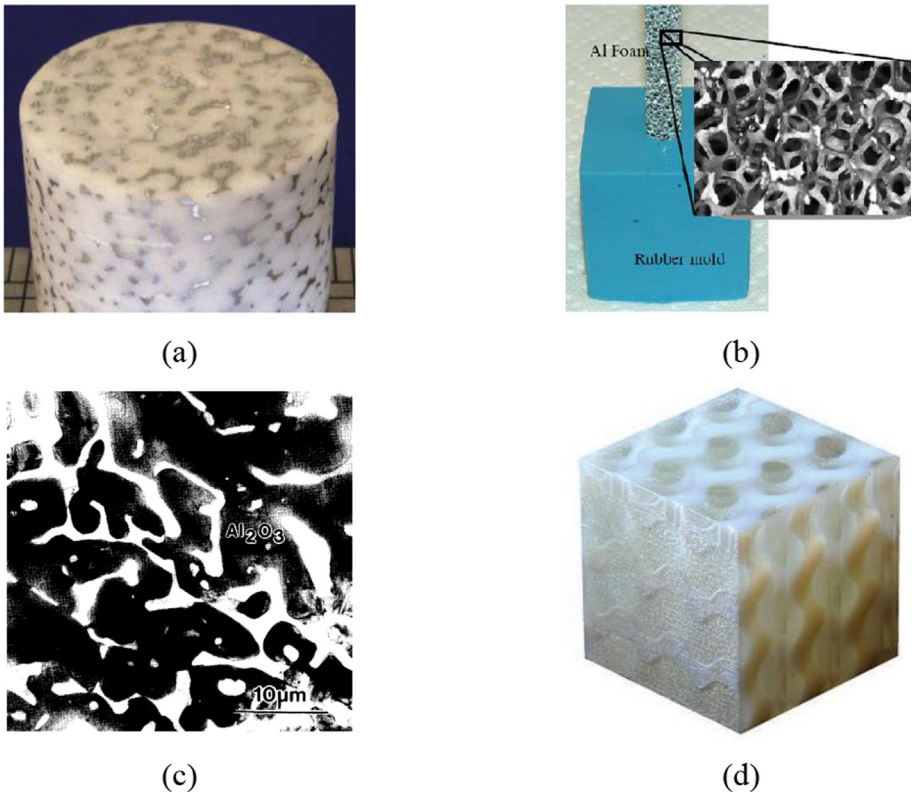

Fig. 11. Different IPCs from literature for comparison. (a) Syntactic Foam with coated aluminium scaffold [22]. (b) Syntactic Foam reinforced by metal foams using open-cell Duocel® aluminium [32]. (c) Al/Al_2O_3 composites [36]. (d) TangoPlus/VeroWhite composites formed by Boolean operations from TPMS [23]. All these results are experimental except Jhaver and Hareesh's work [22].

Table 6
The elastic properties of the constituent materials and the fibre volume fractions in IPCs in literature.

Composites	E_f (MPa)	v_f	E_m (MPa)	v_m	V_f
Syntactic Foam/Al [22]	68,900	0.34	1600	0.33	0.09
Syntactic Foam/Al [32]	69,600	0.35	5122	0.34	0.08
Al/Al_2O_3 [36]	380,000	0.35	69,600	0.25	0.65
TangoPlus/VeroWhite [23]	1660	0.3*	0.7456	0.3*	–
Normalised in simulation [24]	1000	0.33	1.0	0.33	–
TangoPlus/VeroWhite [46]	1660	0.3	0.75	0.3	–

Table 7
Comparison between the normalised Young's moduli of the different types of IPCs in this work and those of the IPCs in literature.

IPCs in literature	E_N			
	Type 1	Type 2	Type 3	Results in literature
Syntactic Foam/Al [22]	0.583	0.378	0.333	0.276
Syntactic Foam/Al [32]	0.761	0.640	0.626	0.602
Al/Al_2O_3 [36]	0.871	0.789	0.791	0.792

TPMS shells and experimentally measured their elastic properties. Dalaq *et al* [24] have used finite element method to simulate the elastic properties of these TPMS-IPCs. The type D of shell TPMS IPCs (D-IPCs) possesses both good mechanical performance and isotropy. Four types of shell TPMS IPCs were also fabricated by 3D printing and the secondary IWP (IWP-S) IPCs have the largest Young's Moduli [46]. Here, the normalised Young's moduli of the D-IPCs obtained by experiments [23] and simulations [24], as well as those of the IWP-S obtained by experiments [46] are compared with the results of our models in Fig. 12(a), (b) and (c), respectively. As can be seen, the IPCs in this paper in general have obviously larger Young's moduli than those reinforced by TPMS shells. For IPCs made of conventional constituent materials (i.e. with constituent materials having positive Poisson's ratios), the IPC reinforced by a cubic fibre-network has a larger Young's modulus than those of all other types of IPCs including the TPMS-IPCs.

It is noted that the composites with their reinforcement phase being a regular cubic closed cell foam of uniform wall thickness [26,30] have an almost isotropic Young's modulus larger than those of all other different types of nearly isotropic composites and have a completely isotropic thermal or electric conductivity that is the same as the theoretical upper limit of all the isotropic composites. The high stiffness of the composites designed in [26] is because regular cubic closed cell foams with a uniform wall thickness have the largest almost isotropic stiffness among all the single-phase cellular materials as confirmed by literature [47], however, the composites in [26] are not IPCs.

5. Conclusion

In this paper, the effects of the constituent materials and the fibre volume fraction on the effective elastic properties of three different types of IPCs are investigated by finite element simulation and analytical methods. It can be concluded from the results that the elastic properties of these of IPCs are almost isotropic, their Young's moduli could be much larger than the Voigt limit, and their Poisson's ratios could be positive, or negative, or zero. This is in line with the analytical results in [26,27]. The normalised Young's moduli of the IPCs depend strongly on the geometrical structure of the reinforcement fibre network, the Poisson's ratios and the ratio of the Young's moduli of the two constituent materials.

In general, the normalised Young's modulus of the IPCs in this paper increases when the ratio E_f/E_m approaches 1 and when the value of $|v_f - v_m|$ increases. When the Poisson's ratios of the two constituent materials are both positive, the normalised Young's modulus of the type-I IPC is larger than those of the other two types of IPCs. In contrast, when the difference of Poisson's ratios of the two constituent materials is large (i.e. v_f is positive and v_m is negative), the normalised Young's modulus of the type-III IPC is larger than that of the type II, and the latter is larger than the type I in most of the cases. The possible reason is that the much larger stiffness of the type-I reinforcement fibre network (i.e. an 'open cell foam') dominates the stiffness of the IPC when the difference of Poisson's ratios of the two constituent materials is small. When the difference of Poisson's ratios of the two constituent materials is large, the stresses and strains in the Type III IPC are more non-uniform, and the much higher stress and strain concentration in the Type III IPC results in larger stored strain energy density and consequently larger stiffness of the IPC. When E_f/E_m is small (e.g. $E_f/E_m = 2$), all three types of IPC are almost isotropic even when the Poisson's ratios of the constituent materials are very different. When E_f/E_m is large, the anisotropy of the IPCs is more dominated by the reinforcement fibre network.

The Young's moduli of the IPCs in this paper are larger than those of their conventional counterparts like particle and short fibre reinforced composites. The theoretical background is that in IPCs, some struts/fibres can directly provide the 'springs-in-paral lel' stiffening mechanism, while the other fibres can enable and enhance the stiffening mechanism or effects of the different Poisson's ratios of the constituent materials. In the particle composites, however, the only stiffening mechanism is the 'springs-in-series' which is much weaker than the 'springs-in-parallel'. Moreover, these three types of IPCs are relatively easy to manufacture, and have an additional mechanism for warning possible failure (e.g. by application of an electric signal). When both the constituent materials are conventional isotropic materials with positive Poisson's ratios, the type-I IPC has the largest Young's modulus among all different types of IPCs including the TPMS-IPCs in [23,24].

Declaration of Competing Interest

The authors declare that they have no known competing financial interests or personal relationships that could have appeared to influence the work reported in this paper.

Appendix I

The geometrical structure shown in Fig. A1 is a 1/8 of the RVE model of the type-I IPC (in Fig. 1a), where l denotes half the edge length of the RVE ($l = L/2$). To simplify the analysis, the self-connected reinforcement fibres are assumed to have a uniform square cross-section with t being half the edge length of the cross-section ($t = T/2$). This 1/8 RVE structure could be used to perform theoretical analysis on the stiffness of the type-I IPCs, and the structure can be divided into 8 parallelepipeds. When the IPC is stretched by a strain ε_x in the $\times$ direction, according to the structural symmetry, the normal stress components in the parallelepipeds are denoted as $\sigma_{x1}, \sigma_{x2}, \sigma_{x3}, \sigma_{y1}, \sigma_{y2}, \sigma_{y3}$ and σ_{y4}, and the corresponding lateral strain is denoted as ε_y.

The force equilibrium and the deformation compatibility conditions require the following relations to be satisfied:

$$\frac{l-t}{lE_B}\left(\sigma_{x1} - v_B\sigma_{y1} - v_B\sigma_{y4}\right) + \frac{t}{lE_A}\left(\sigma_{x1} - v_A\sigma_{y2} - v_A\sigma_{y3}\right) = \varepsilon_x \quad \text{(A1)}$$

$$\frac{l-t}{lE_A}\left(\sigma_{x2} - 2v_A\sigma_{y1}\right) + \frac{t}{lE_A}\left(\sigma_{x2} - 2v_A\sigma_{y2}\right) = \varepsilon_x \quad \text{(A2)}$$

$$\frac{l-t}{lE_B}\left(\sigma_{x3} - 2v_B\sigma_{y4}\right) + \frac{t}{lE_B}\left(\sigma_{x3} - 2v_B\sigma_{y3}\right) = \varepsilon_x \quad \text{(A3)}$$

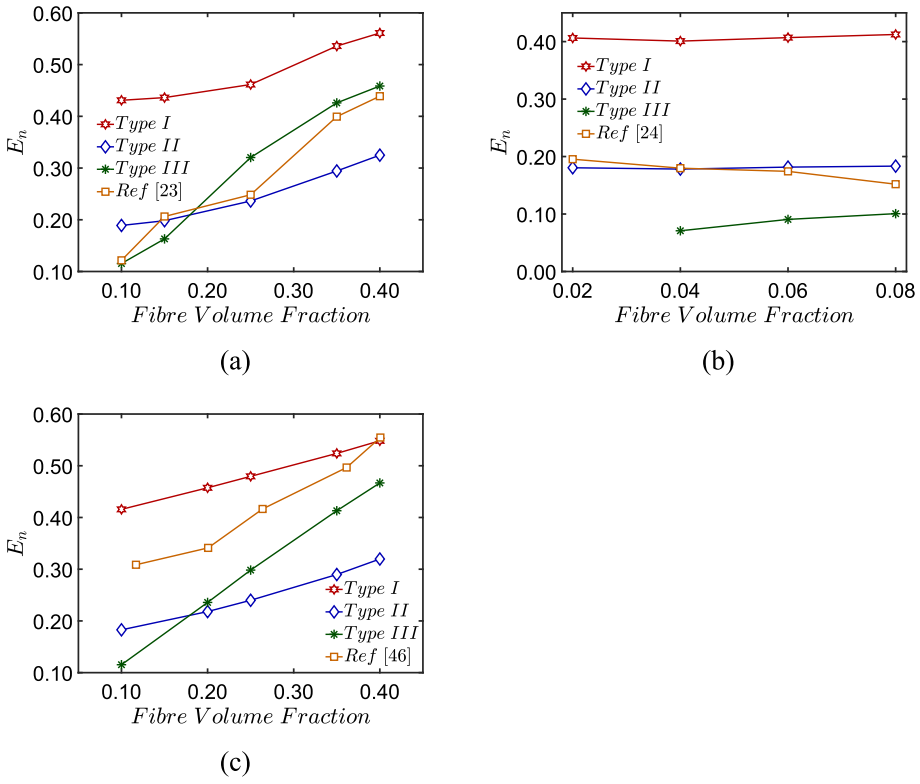

Fig. 12. Comparison between the normalised Young's moduli of the three types of IPCs in this paper and the IPCs reinforced by different types of TPMS shells in (a) Ref. [23], (b) Ref. [24], (c) Ref. [46].

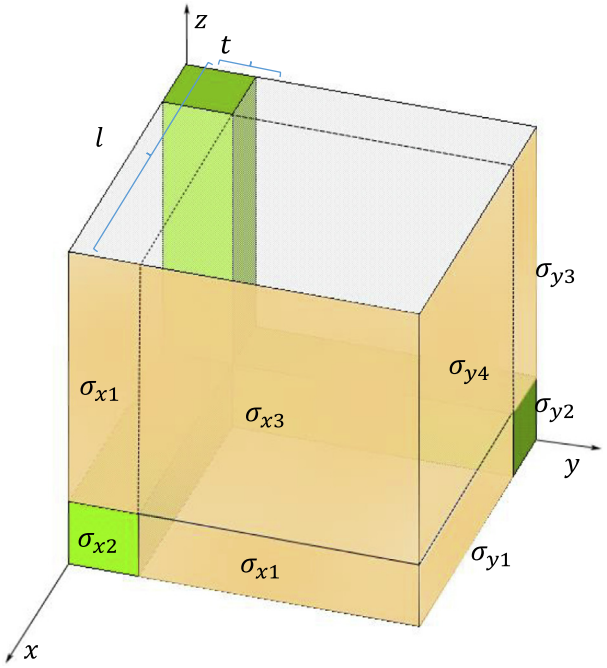

Fig. A1. 1/8 RVE of the type-I IPCs for theoretical analysis.

$$\frac{l-t}{lE_B}(\sigma_{y1}-\nu_B\sigma_{x1}-\nu_B\sigma_{y4})+\frac{t}{lE_A}(\sigma_{y1}-\nu_A\sigma_{x2}-\nu_A\sigma_{y1})=\varepsilon_y \tag{A4}$$

$$\frac{l-t}{lE_A}(\sigma_{y2}-\nu_A\sigma_{x1}-\nu_A\sigma_{y3})+\frac{t}{lE_A}(\sigma_{y2}-\nu_A\sigma_{y2}-\nu_A\sigma_{x2})=\varepsilon_y \tag{A5}$$

$$\frac{l-t}{lE_B}(\sigma_{y3}-\nu_B\sigma_{x3}-\nu_B\sigma_{y3})+\frac{t}{lE_A}(\sigma_{y3}-\nu_A\sigma_{x1}-\nu_A\sigma_{y2})=\varepsilon_y \tag{A6}$$

$$\frac{l-t}{lE_B}(\sigma_{y4}-\nu_B\sigma_{y4}-\nu_B\sigma_{x3})+\frac{t}{lE_B}(\sigma_{y4}-\nu_B\sigma_{x1}-\nu_B\sigma_{y1})=\varepsilon_y \tag{A7}$$

$$(l-t)^2\sigma_{y4}+(l-t)t\sigma_{y1}+(l-t)t\sigma_{y3}+t^2\sigma_{y2}=0 \tag{A8}$$

The 7 unknown normal stress components and the lateral stress ε_y can be determined by solving the above 8 simultaneous equations. Thus, the effective Young's modulus and the Poisson's ratio of the IPC can be obtained.

Appendix II

The von Mise stress contour images of the deformed RVEs of the type I and III IPCs are provided here for comparison, where $E_f = 2$, $E_m = 1$ and the uniaxial tensile strain $\varepsilon_x = 0.001$ (see Fig. A2).

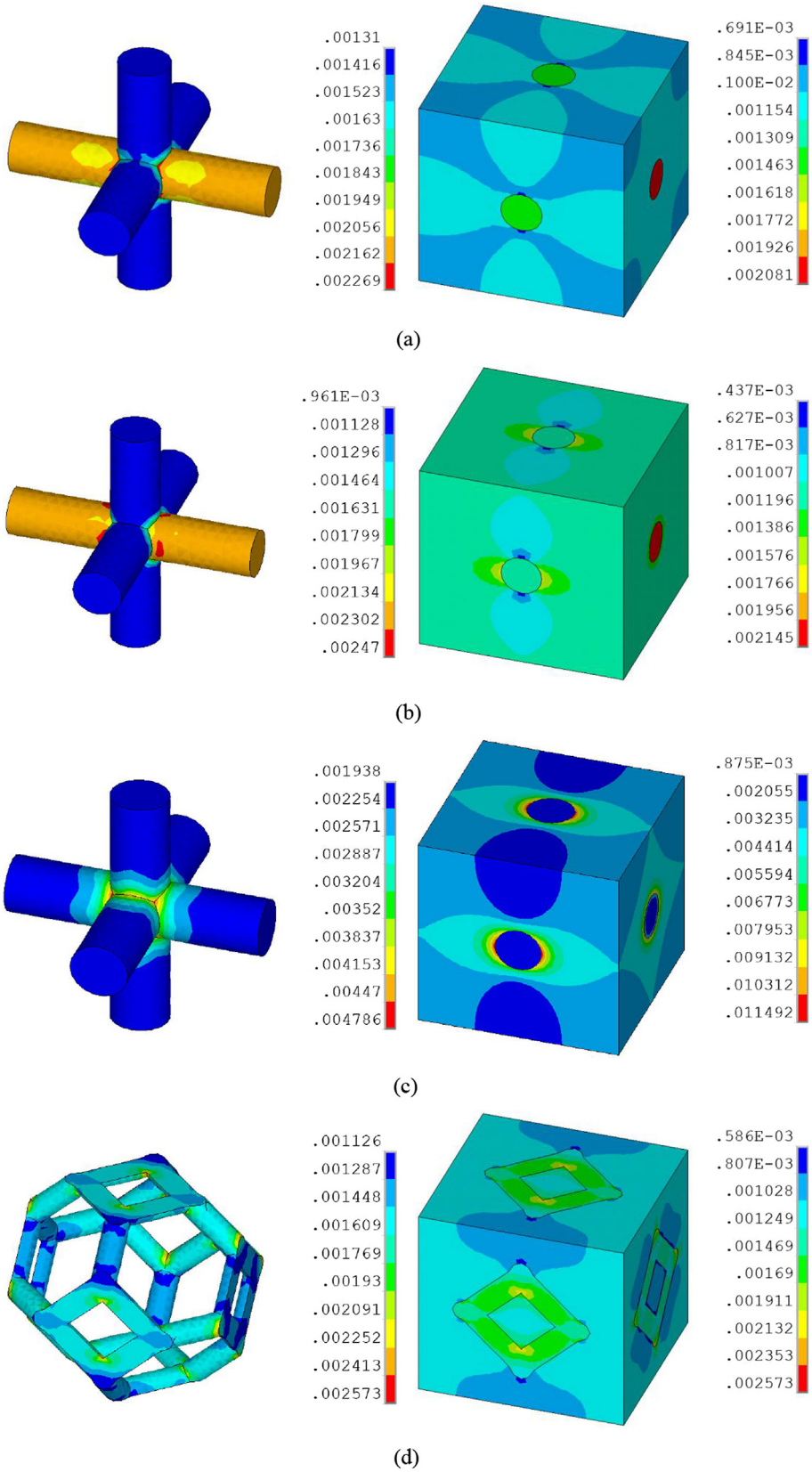

Fig. A2. The von Mises stress contour images of the deformed RVEs with $E_m = 1$, $E_f/E_m = 2$. (a) Type I, $v_f = v_m = 0.3$. (b) Type I, $v_f = 0.49$, $v_m = 0.05$. (c) Type I, $v_f = 0.49$, $v_m = -0.8$. (d) Type III, $v_f = v_m = 0.3$. (e) Type III, $v_f = 0.49$, $v_m = 0.05$. (f) Type III, $v_f = 0.49$, $v_m = -0.8$.

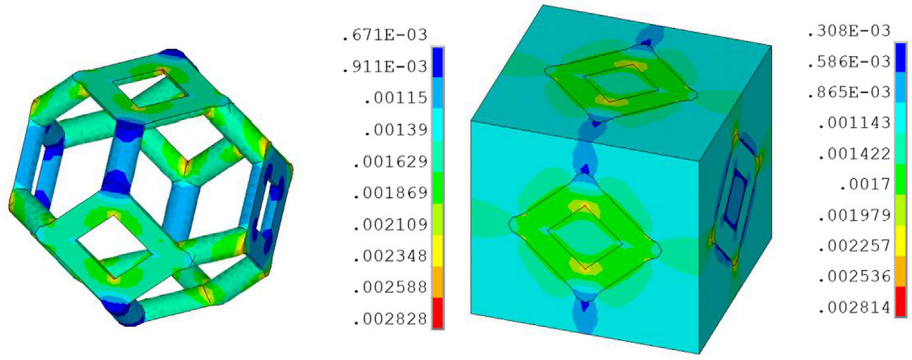

(e)

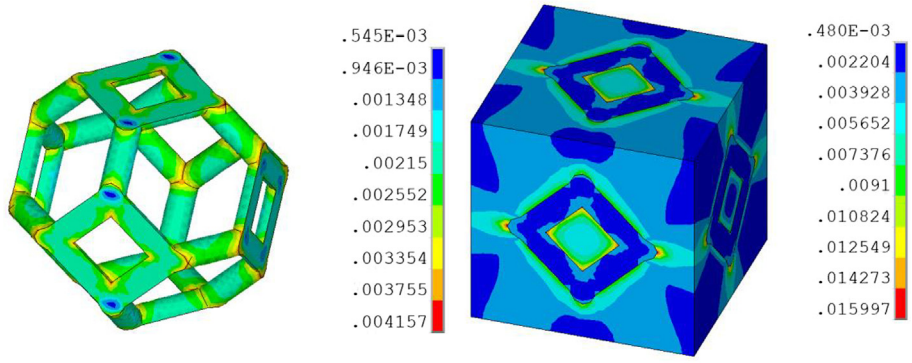

(f)

Fig. A2 (*continued*)

References

[1] D.R. Clarke, Interpenetrating phase composites, J. Am. Ceram. Soc. 75 (1992) 739–758, https://doi.org/10.1111/j.1151-2916.1992.tb04138.x.

[2] M.E. Umanzor, R.C. Batra, C.B. Williams, A.P. Druschitz, Penetration resistance of cast metal-ceramic composite lattice structures, Adv. Eng. Mater. 23 (2021) 1–13, https://doi.org/10.1002/adem.202100577.

[3] W. Huang, M. Shishehbor, N. Guarín-Zapata, N.D. Kirchhofer, J. Li, L. Cruz, T. Wang, S. Bhowmick, D. Stauffer, P. Manimunda, K.N. Bozhilov, R. Caldwell, P. Zavattieri, D. Kisailus, A natural impact-resistant bicontinuous composite nanoparticle coating, Nat. Mater. 19 (2020) 1236–1243, https://doi.org/10.1038/s41563-020-0768-7.

[4] Y. Zhang, M.-T. Hsieh, L. Valdevit, Mechanical performance of 3D printed interpenetrating phase composites with spinodal topologies, Compos. Struct. 263 (2021) 113693, https://doi.org/10.1016/j.compstruct.2021.113693.

[5] M. Frey, L. Schneider, K. Masania, T. Keplinger, I. Burgert, Delignified wood-polymer interpenetrating composites exceeding the rule of mixtures, ACS Appl. Mater. Interf. 11 (2019) 35305–35311, https://doi.org/10.1021/acsami.9b11105.

[6] M.T. Hsieh, M.R. Begley, L. Valdevit, Architected implant designs for long bones: advantages of minimal surface-based topologies, Mater. Des. 207 (2021) 109838, https://doi.org/10.1016/j.matdes.2021.109838.

[7] J. Li, J. Li, Q. Zhao, R. Xia, Molecular dynamics simulations on the mechanical properties of gyroidal bicontinuous Cu/Ni nanocomposites, J. Mater. Res. Technol. 18 (2022) 4738–4747, https://doi.org/10.1016/j.jmrt.2022.04.142.

[8] Y. Wang, D. Lu, W. Ma, Y. Zhang, Compression and wear properties of ultrafine Al2O3p/iron composites prepared by cast infiltration, Jom 74 (2022) 1878–1885, https://doi.org/10.1007/s11837-022-05237-9.

[9] L. Chen, B. Li, L. Zhu, X. Deng, X. Sun, Y. Liu, C. Zhang, W. Zhao, X. Chen, A PVA/LiCl/PEO interpenetrating composite electrolyte with a three-dimensional dual-network for all-solid-state flexible aluminum-air batteries, RSC Adv. 11 (2021) 39476–39483, https://doi.org/10.1039/d1ra07180g.

[10] M. Zhang, Q. Yu, Z. Liu, J. Zhang, G. Tan, D. Jiao, W. Zhu, S. Li, Z. Zhang, R. Yang, R.O. Ritchie, 3D printed Mg-NiTi interpenetrating-phase composites with high strength, damping capacity, and energy absorption efficiency, Sci. Adv. 6 (2020) 1–10, https://doi.org/10.1126/sciadv.aba5581.

[11] C. Zhou, Y. Zhou, Q. Zhang, Q. Meng, L. Zhang, E. Kobayashi, G. Wu, Near-zero thermal expansion of ZrW2O8/Al–Si composites with three dimensional interpenetrating network structure, Compos. Part B Eng. 211 (2021) 108678, https://doi.org/10.1016/j.compositesb.2021.108678.

[12] S. Rawal, Metal-matrix composites for space applications, Jom. 53 (2001) 14–17, https://doi.org/10.1007/s11837-001-0139-z.

[13] G.B.V. Kumar, C.S.P. Rao, N. Selvaraj, Mechanical and tribological behavior of particulate reinforced aluminum metal matrix composites – a review, J. Miner. Mater. Charact. Eng. 10 (2011) 59–91, https://doi.org/10.4236/jmmce.2011.101005.

[14] Z. Sadeghian, B. Lotfi, M.H. Enayati, P. Beiss, Microstructural and mechanical evaluation of Al-TiB2 nanostructured composite fabricated by mechanical alloying, J. Alloys Compd. 509 (2011) 7758–7763, https://doi.org/10.1016/j.jallcom.2011.04.145.

[15] S. Bathula, M. Saravanan, A. Dhar, Nanoindentation and wear characteristics of Al 5083/SiCp nanocomposites synthesized by high energy ball milling and spark plasma sintering, J. Mater. Sci. Technol. 28 (2012) 969–975, https://doi.org/10.1016/S1005-0302(12)60160-1.

[16] J. Verma, A. Kumar, R. Chandrakar, R. Kumar, Processing of 5083 aluminum alloy reinforced with alumina through microwave sintering, J. Miner. Mater. Charact. Eng. 11 (2015) 1126–1131, https://doi.org/10.4236/jmmce.2012.1111121.

[17] M. Li, K. Ma, L. Jiang, H. Yang, E.J. Lavernia, L. Zhang, J.M. Schoenung, Synthesis and mechanical behavior of nanostructured Al 5083/n-TiB2 metal matrix composites, Mater. Sci. Eng. A. 656 (2016) 241–248, https://doi.org/10.1016/j.msea.2016.01.031.

[18] E.B.V. All, High damping capacity of AlSi10Mg-NiTi lattice structure interpenetrating phase composites prepared by additive manufacturing and pressureless infiltration, J. Alloys Compd. 905 (2022) 164075, https://doi.org/10.1016/j.jallcom.2022.164075.

[19] X. Chen, Y. Wu, H. Liu, Y. Wang, G. Zhao, Q. Zhang, F. Wang, Y. Liu, Mechanical performance of PEEK-Ti6Al4V interpenetrating phase composites fabricated by powder bed fusion and vacuum infiltration targeting large and load-bearing implants, Mater. Des. 215 (2022) 110531, https://doi.org/10.1016/j.matdes.2022.110531.

[20] F. Xie, Z. Lu, Z. Yuan, Numerical analysis of elastic and elastoplastic behavior of interpenetrating phase composites, Comput. Mater. Sci. 97 (2015) 94–101, https://doi.org/10.1016/j.commatsci.2014.10.021.

[21] Z. Poniznik, V. Salit, M. Basista, D. Gross, Effective elastic properties of interpenetrating phase composites, Comput. Mater. Sci. 44 (2008) 813–820, https://doi.org/10.1016/j.commatsci.2008.06.010.

[22] R. Jhaver, H. Tippur, Processing, compression response and finite element modeling of syntactic foam based interpenetrating phase composite (IPC), Mater. Sci. Eng. A. 499 (2009) 507–517, https://doi.org/10.1016/j.msea.2008.09.042.

[23] O. Al-Ketan, R.K.A. Al-Rub, R. Rowshan, Mechanical properties of a new type of architected interpenetrating phase composite materials, Adv. Mater. Technol. 2 (2017) 1600235, https://doi.org/10.1002/admt.201600235.

[24] A.S. Dalaq, D.W. Abueidda, R.K. Abu Al-Rub, I.M. Jasiuk, Finite element prediction of effective elastic properties of interpenetrating phase composites with architectured 3D sheet reinforcements, Int. J. Solids Struct. 83 (2016) 169–182, https://doi.org/10.1016/j.ijsolstr.2016.01.011.
[25] D.W. Abueidda, R.K. Abu Al-Rub, A.S. Dalaq, D.W. Lee, K.A. Khan, I. Jasiuk, Effective conductivities and elastic moduli of novel foams with triply periodic minimal surfaces, Mech. Mater. 95 (2016) 102–115, https://doi.org/10.1016/j.mechmat.2016.01.004.
[26] H.X. Zhu, T.X. Fan, D. Zhang, Composite materials with enhanced dimensionless Young's modulus and desired Poisson's ratio, Sci. Rep. 5 (2015) 1–8, https://doi.org/10.1038/srep14103.
[27] H. Zhu, T. Fan, C. Xu, D. Zhang, Nano-structured interpenetrating composites with enhanced Young's modulus and desired Poisson's ratio, Compos. Part A Appl. Sci. Manuf. 91 (2016) 195–202, https://doi.org/10.1016/j.compositesa.2016.10.006.
[28] Z. Zhang, H. Zhu, R. Yuan, S. Wang, T. Fan, Y. Rezgui, D. Zhang, Auxetic interpenetrating composites: A new approach to non-porous materials with a negative or zero Poisson's ratio, Compos. Struct. 243 (2020) 112195, https://doi.org/10.1016/j.compstruct.2020.112195.
[29] T. Li, Y. Chen, X. Hu, Y. Li, L. Wang, Exploiting negative Poisson's ratio to design 3D-printed composites with enhanced mechanical properties, Mater. Des. 142 (2018) 247–258, https://doi.org/10.1016/j.matdes.2018.01.034.
[30] H. Zhu, T. Fan, D. Zhang, Composite materials with enhanced conductivities, Adv. Eng. Mater. 18 (2016) 1174–1180, https://doi.org/10.1002/adem.201500482.
[31] S.Y. Fu, X.Q. Feng, B. Lauke, Y.W. Mai, Effects of particle size, particle/matrix interface adhesion and particle loading on mechanical properties of particulate-polymer composites, Compos. Part B Eng. 39 (2008) 933–961, https://doi.org/10.1016/j.compositesb.2008.01.002.
[32] C. Periasamy, H.V. Tippur, Experimental measurements and numerical modeling of dynamic compression response of an interpenetrating phase composite foam, Mech. Res. Commun. 43 (2012) 57–65, https://doi.org/10.1016/j.mechrescom.2012.03.002.
[33] G.S. Daehn, B. Starck, L. Xu, K.F. Elfishawy, J. Ringnalda, H.L. Fraser, Elastic and plastic behavior of a co-continuous alumina/aluminum composite, Acta Mater. 44 (1996) 249–261, https://doi.org/10.1016/1359-6454(95)00138-8.
[34] I.M. Gitman, H. Askes, L.J. Sluys, Representative volume: existence and size determination, Eng. Fract. Mech. 74 (2007) 2518–2534, https://doi.org/10.1016/j.engfracmech.2006.12.021.
[35] G.W. Milton, Composite materials with Poisson's ratios close to - 1, J. Mech. Phys. Solids. 40 (1992) 1105–1137, https://doi.org/10.1016/0022-5096(92)90063-8.
[36] M.C. Breslin, J. Ringnalda, L. Xu, M. Fuller, J. Seeger, G.S. Daehn, T. Otani, H.L. Fraser, Processing, microstructure, and properties of co-continuous alumina-aluminum composites, Mater. Sci. Eng. A. 195 (1995) 113–119.
[37] L.J. Gibson, M.F. Ashby, Cellular Solids: Structure and Properties, Cambridge University Press, 1999. <https://books.google.co.uk/books?id=rzVIBAAAQBAJ>.
[38] G.N. Greaves, A.L. Greer, R.S. Lakes, T. Rouxel, Poisson's ratio and modern materials, Nat. Mater. 10 (2011) 823–837, https://doi.org/10.1038/nmat3134.
[39] H.X. Zhu, J.F. Knott, N.J. Mills, Analysis of the elastic properties of open-cell foams with tetrakaidecahedral cells, J. Mech. Phys. Solids. 45 (1997) 319–343, https://doi.org/10.1016/S0022-5096(96)00090-7.
[40] H.X. Zhu, J.R. Hobdell, A.H. Windle, Effects of cell irregularity on the elastic properties of open-cell foams, Acta Mater. 48 (20) (2000) 4893–4900.
[41] R. Lakes, Foam structures with a negative Poisson's ratio, Science (80-) 235 (4792) (1987) 1038–1040.
[42] ANSYS® Academic Research Mechanical, Release 16.0., (n.d.).
[43] N. Chawla, R.S. Sidhu, V.V. Ganesh, Three-dimensional visualization and microstructure-based modeling of deformation in particle-reinforced composites, Acta Mater. 54 (2006) 1541–1548, https://doi.org/10.1016/j.actamat.2005.11.027.
[44] M.E.J. Dekkers, D. Heikens, The effect of interfacial adhesion on the tensile behavior of polystyrene–glass-bead composite, J. Appl. Polym. Sci. 28 (1983) 3809–3815.
[45] C.-E. Rousseau, H. Tippur, Compositionally graded materials with cracks normal to the elastic gradient, Acta Mater. 48 (2000) 4021–4033, https://doi.org/10.1016/S1359-6454(00)00202-0.
[46] M. Al-Ketan, R.K.A. Adel, M.A. Al-rub, R.K. Assad, Abu Al-Rub, Mechanical properties of periodic interpenetrating phase composites with novel architected microstructures, Compos. Struct. 176 (2017) 9–19, https://doi.org/10.1016/j.compstruct.2017.05.026.
[47] J.B. Berger, H.N.G. Wadley, R.M. McMeeking, Mechanical metamaterials at the theoretical limit of isotropic elastic stiffness, Nature 543 (2017) 533–537, https://doi.org/10.1038/nature21075.